

Synthesis and Characterization of M-doped $\text{Li}_{1.05}\text{Co}_{0.3}\text{Ni}_{0.35}\text{Mn}_{0.3}\text{O}_2$ (M=Zn, Fe, Ti, Zr) Cathode Materials for Lithium ion Battery

Yuhong Chen

Department of Chemical and Environmental Engineering, Hebei Chemical & Pharmaceutical Vocational Technology College, Shijiazhuang 050026, China
E-mail: chyh76@163.com

Received: 6 February 2022 / Accepted: 18 March 2022 / Published: 5 April 2022

In order to improve the electrochemical properties and thermal stability of $\text{Li}_{1.05}\text{Co}_{1/3}\text{Ni}_{1/3}\text{Mn}_{1/3}\text{O}_2$ materials. $\text{Li}_{1.05}\text{Co}_{0.3}\text{Ni}_{0.35}\text{Mn}_{0.3}\text{M}_{0.05}\text{O}_2$ (M=Zn, Fe, Ti, Zr) materials were prepared by co-precipitation method. The structure, morphology, electrochemical performance and thermal stability were studied by XRD, ESEM, cyclic voltammetry (CV), charge-discharge cycling, electrochemical impedance spectroscopy (EIS) and DSC. Results showed that all materials had stable layered structure with a-NaFeO₂. However, the impurity peaks of ZnO appeared in Zn-doping materials, ZnO did not take part in the electrochemical reactions and did not affect the electrochemical properties of the materials. The impurity peaks Li_2MnO_3 appeared in Fe-doping materials, Li_2MnO_3 took part in the electrochemical reaction and affected the electrochemical properties of the materials. The doping of Zn^{2+} , Zr^{4+} or Ti^{4+} (especially Ti^{4+}) can improve the dynamic properties of the materials. The order of rate performance and cyclic stability at 1C rate current was Ti^{4+} -doped > Zr^{4+} -doped > Zn^{2+} -doped > no doped > Fe^{3+} -doped. The thermal stability order of the materials was Ti^{4+} -doped > Zr^{4+} -doped > Zn^{2+} -doped > Fe^{3+} -doped = no doped.

Keywords: cathode materials; $\text{LiCo}_{1/3}\text{Ni}_{1/3}\text{Mn}_{1/3}\text{O}_2$ co-precipitation lithium-ion batteries;

1. INTRODUCTION

Recently layer $\text{LiNi}_{1/3}\text{Mn}_{1/3}\text{Co}_{1/3}\text{O}_2$ materials have become a research hotspot because of their higher capacity and better security [1]. However, it has some disadvantages, such as lower discharge capacity at high current and lower thermal stability than LiFePO_4 , lower cyclic stability than LiCoO_2 , difficult to control the morphology of particles in the synthesis process [2-5]. One of the ways to improve the materials performance was to use transition metal or non-transition metal doping. It was reported that transition metal doping included Fe [6], Ti [7], Zr [8], Zn [9], Mo [10], Cr [11] doping, and non-transition

metal doping included Al[8,12] and Mg doping[13]. Some metal dopants may stabilize the layered structure and prevent unnecessary reactions between the cathode and the electrolyte, whether or not involved in the oxidation-reduction process.

So far as I know, although there were some reports on Li-Co-Ni-Mn oxides doped with a single element, such as Zn^{2+} , Fe^{3+} , Ti^{4+} , Zr^{4+} . But almost no one has synthesized and compared four element-doped materials at the same time. In this paper, four kinds of doping materials were prepared and their morphology, structures, electrochemical properties and thermal stability were compared too.

2. EXPERIMENTAL

2.1 Preparation of $Li_{1.05}Co_{0.3}Ni_{0.35}Mn_{0.3}M_{0.05}O_2$ ($M=Zn, Fe, Ti, Zr$)

The precursor $Co_{0.3}Ni_{0.4-x}Mn_{0.3}(OH)_2$ was prepared by co-precipitation method. According to the stoichiometry, a mixture of cobalt, nickel and manganese sulfates was prepared in 0.25 mol/l. The mixed solution and 0.5 mol/l NaOH solution were put into two burets and slowly dripped into the reaction vessel under stirring condition at 45-50°C. In the reaction process, the reaction time was controlled by the dropping speed and the pH value (11-11.5) was controlled by the amount of NH_4OH . After filtering, washing, drying and grinding, the precursor was obtained.

The lithium hydroxide, the precursor, and the doped metal oxides were ground and mixed in accordance with the stoichiometry. The milled mixture was calcined in a muffle furnace at 500°C for 4 hours and at 900°C for 8 hours to obtain $Li_{1.05}Co_{0.3}Ni_{0.35}Mn_{0.3}M_{0.05}O_2$ ($M=Zn, Fe, Ti, Zr$) materials.

2.2 Preparation of experimental batteries

The 2032 battery was used as the experimental battery. The ratio of cathode materials slurry was active substance, carbon black and PTFE (85:5:5 in weight). The slurry was extruded onto the Al foil, electrodes with an area of 0.5cm^2 and a depth of 0.02mm were made and dried 12h at 120 °C in vacuum drier. 2032 batteries were made in a nitrogen filled dry box with Li metal as counter electrodes, celgard 2400 as separators and 1M $LiPF_6$ in EC/EMC/DMC (1:1:1 in weight) as electrolyte.

2.3 Structure and morphology tests

The materials morphology was tested by ESEM (Philips XL-30). XRD (Philips X' Pert Pro MPD Co-K α) was used to study the structure.

2.4 Electrochemical performance tests

Cyclic voltammetry (CV) and AC impedance were measured using electrochemical instruments (Gamry instruments). The CCCV charge was enforced at different rate between 2.75V-4.3V.

2.5 DSC tests

In N₂-filled dry box, the charging to 4.3V batteries were opened and the excess electrolytes from the electrode surface was removed by DMC washing. 3–5 mg cathode materials were scraped off the foil and collected in an aluminum sealed plate. Thermal stability was measured by a differential scanning calorimeter (netzsch-204) at a scanning rate of 10°C/min.

3. RESULTS AND DISCUSSION

3.1 Structural properties

XRD spectra of Li_{1.05}Co_{0.3}Ni_{0.35}Mn_{0.3}M_{0.05}O₂ (M=Zn、Fe、Ti、Zr) were shown in Fig.1. All of the graphs showed patterns indexable in the a-NaFeO₂ layered structure with space group *R-3m*[14].

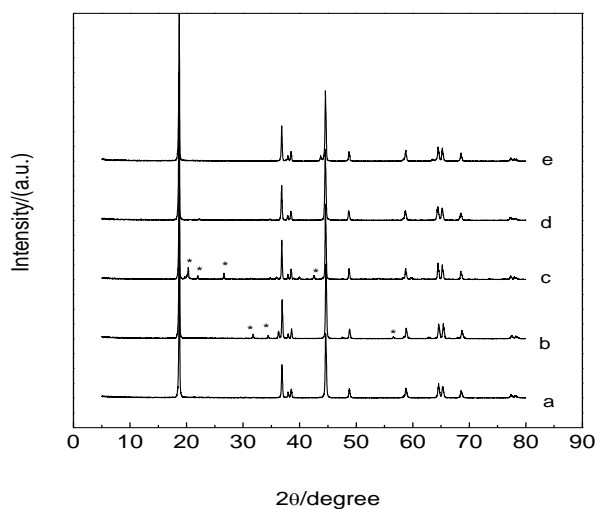


Figure 1. XRD spectra of Li_{1.05}Co_{0.3}Ni_{0.35}Mn_{0.3}M_{0.05}O₂ (M=Zn、Fe、Ti、Zr) materials (a) no doped,(b)Zn²⁺-doped,(c) Fe³⁺-doped,(d) Ti⁴⁺- doped,(e) Zr⁴⁺-doped,* Stands for impurity peak

Table 1. Lattice parameters of the transition metal cation doped samples

Samples	c	a	c/a	Volume	R	$\Delta\theta_1$	$\Delta\theta_2$
Black	14.2086	2.8562	4.9747	100.3828	1.48	0.542	0.703
Zn ²⁺ -doped	14.2098	2.8526	4.9814	100.1383	1.44	0.581	0.819
Fe ³⁺ -doped	14.2224	2.8585	4.9756	100.6422	1.41	0.561	0.761
Ti ⁴⁺ -doped	14.2392	2.8572	4.9836	100.6694	1.52	0.562	0.799
Zr ⁴⁺ -doped	14.2233	2.8584	4.9760	100.6415	1.49	0.56	0.757

$\Delta\theta_2$ represented the splitting degree between (006) and (102) double peaks, $\Delta\theta_1$ represented the splitting degree between (1 0 8) and (1 1 0) double peaks, *R* denoting the ratio I_{003}/I_{104} .

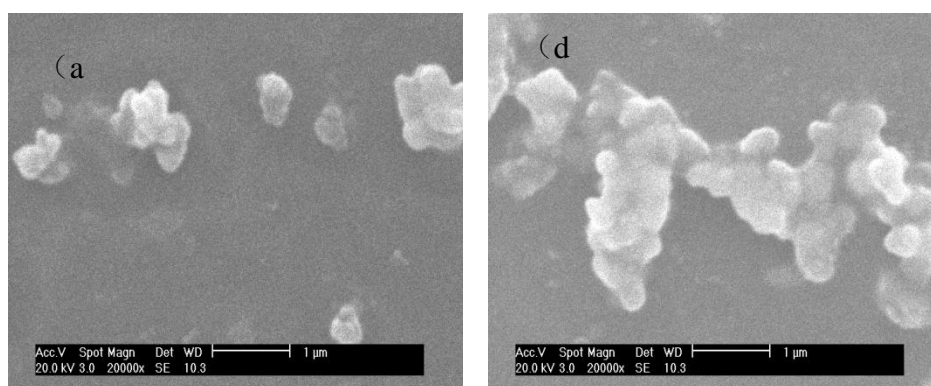
Table1 showed the the hexagonal lattice parameters calculating by a least squares method.As shown in Fig.1 and Table 1, the (006) and (102) peaks and (108) and (110) peaks were obviously split,

and the ratio of I_{003}/I_{104} were relatively large, which showed that the doped samples still maintained a good layered structure.

It was shown from Fig. 1b and Table 1 that Zn^{2+} -doped samples have impurity peaks at $30-40^\circ$, 47.5° and 56.6° , which may be the impurity peaks of ZnO. The appearance of the impurity peaks was due to the high doping amount of Zn^{2+} . When the doping amount was less than 0.01, no impurity peak appears [13,15]. Compared with the unadulterated samples, the lattice constant c of Zn^{2+} -doped samples increased slightly and the lattice constant a decreased, so the ratio of c to a went up and the volume went down, which indicated that the layered materials after Zn^{2+} -doping had a more stable structure. Although the ion radius of Zn^{2+} was larger than that of Co^{3+} , Ni^{3+} or Mn^{3+} , the volume of Zn^{2+} -doped samples decreased. The reason may be that part of Zn^{2+} replaced Li^+ , or part of Zn^{2+} replaced the position of transition metal, which compensated for the defect of transition metals and made the layer structure more compact [16].

It was shown from Fig. 1b and Table 1 that Zn^{2+} -doped samples have impurity peaks at $30-40^\circ$, 47.5° and 56.6° , which may be the impurity peaks of ZnO. The appearance of the impurity peaks was due to the high doping amount of Zn^{2+} . When the doping amount was less than 0.01, no impurity peak appears [13,15]. Compared with the unadulterated samples, the lattice constant c of Zn^{2+} -doped samples increased slightly and the lattice constant a decreased, so the value of c/a increased and the volume decreased, which indicated that the layered materials after Zn^{2+} -doping has a more stable structure. Although the ion radius of Zn^{2+} was larger than that of Co^{3+} , Ni^{3+} or Mn^{3+} , the volume of Zn^{2+} -doped samples decreased. The reason may be that part of Zn^{2+} replaced Li^+ , or part of Zn^{2+} replaced the position of transition metal, which compensated for the defect of transition metals and made the layer structure more compact [16].

Fig. 1c and table 1 showed that the Fe^{3+} doped samples had a impurity peak between $20-25^\circ$, which may be the peak of Li_2MnO_3 [17]. The appearance of impurity peaks made the materials unable to form good homogeneous co-solution, which may lead to the deterioration of electrochemical properties. At the same time, it showed that c and a increased and the volume expanded slightly, the ratio of I_{003}/I_{104} decreased, which was due to Fe^{3+} replaced the transition metal positions and the larger ionic radius of Fe^{3+} than that of Co^{3+} , Ni^{3+} or Mn^{3+} . Volume expansion may also lead to deterioration of electrochemical properties [18,19].



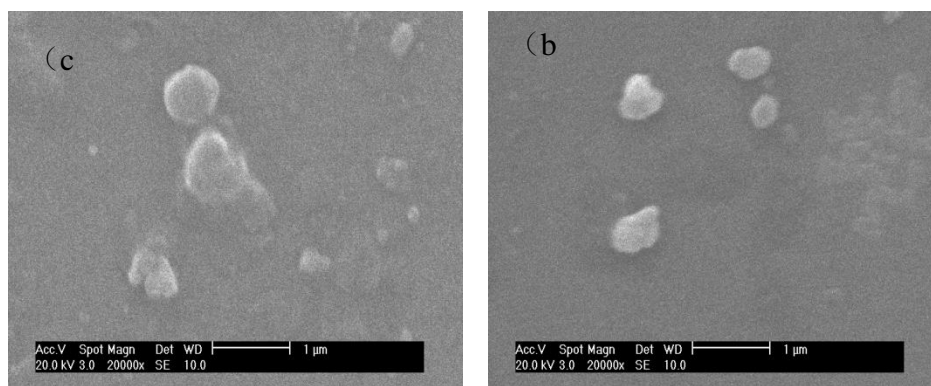


Figure 2. ESEM photograph of $\text{Li}_{1.05}\text{Co}_{0.3}\text{Ni}_{0.35}\text{Mn}_{0.3}\text{M}_{0.05}\text{O}_2$ ($\text{M}=\text{Zn}, \text{Fe}, \text{Ti}, \text{Zr}$) materials (a) Zn^{2+} -doped, (b) Fe^{3+} -doped, (c) Ti^{4+} -doped (d) Zr^{4+} -doped

No impurity peaks can be found in Ti^{4+} and Zr^{4+} doped samples, which indicated that the samples can form good homogeneities. As the radii of Ti^{4+} and Zr^{4+} are larger than those of Co^{3+} , Ni^{3+} or Mn^{3+} , the lattice parameters c and a of the doped samples increased. The increasing c/a value of Ti^{4+} and Zr^{4+} doped samples indicated that the layered structure of the doped samples was more compact and stable. The increase of I_{003}/I_{104} ratio of Ti^{4+} and Zr^{4+} doped materials indicated that the cation arrangement of doped samples was more orderly. The substitution of Ti^{4+} and Zr^{4+} for transition metals led to the rearrangement of cation in the crystal structure and the change of crystal structure, which ultimately affected electrical properties and safety of the materials[20, 21].

3.2 Cyclic voltammetry

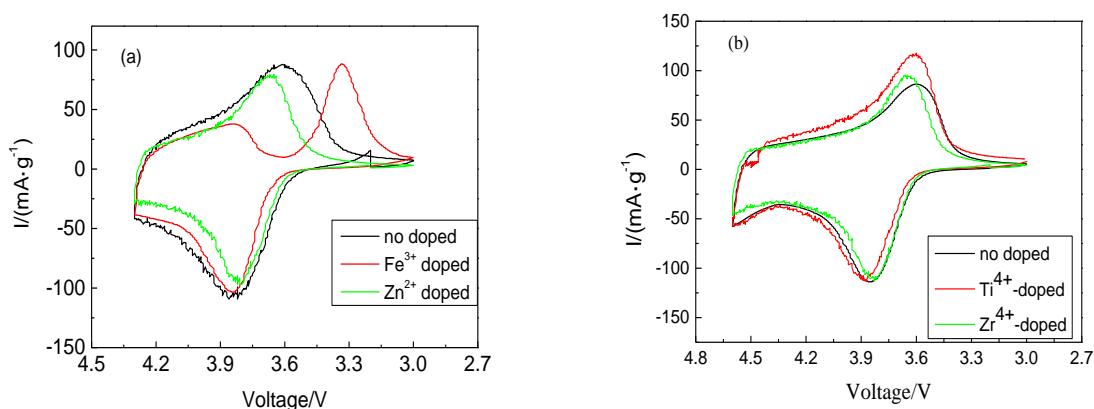


Figure 3. Cyclic voltammery of $\text{Li}_{1.05}\text{Co}_{0.3}\text{Ni}_{0.35}\text{Mn}_{0.3}\text{M}_{0.05}\text{O}_2$ ($\text{M}=\text{Zn}, \text{Fe}, \text{Ti}, \text{Zr}$) electrodes

Fig. 3 showed the cyclic voltammograms of $\text{Li}_{1.05}\text{Co}_{0.3}\text{Ni}_{0.35}\text{Mn}_{0.3}\text{M}_{0.05}\text{O}_2$ ($\text{M} = \text{Zn}, \text{Fe}, \text{Ti}, \text{Zr}$) electrodes at room temperature at 0.1 mv/s sweep rate. Fig.3a showed that the undoped samples and the Zn^{2+} doped samples only had a pair of redox peaks in the range of 3.0-4.3 V, which correspond to $\text{Ni}^{2+}/\text{Ni}^{4+}$ redox pairs [14], but the Fe^{3+} -doped samples showed two reduction peaks at 3.9V and 3.3V. The reduction peak at 3.9V was $\text{Ni}^{4+}/\text{Ni}^{2+}$ and the latter one was $\text{Mn}^{4+}/\text{Mn}^{3+}$ [14]. The latter one was caused

by Li_2MnO_3 impurity phase, which was consistent with the XRD test. This indicated that the impurity ZnO produced by Zn^{2+} doping was an inert materials, which will not destroy the redox reaction of the cathode materials and will not cause too much negative impact on the electrochemical properties. However, the impurity Li_2MnO_3 causing by Fe^{3+} doping participated in the electrochemical reaction, thus affected the electrochemical stability of the raw materials. Fig. 3a also showed that Zn^{2+} doping shifted the reduction peak potential to the left and the difference of reduction-oxidation peak potential reduced, which suggested that Zn^{2+} doping may decrease the electric polarization during charging and discharging process. The oxidation and reduction peak areas of samples doped with Zn^{2+} and Fe^{3+} were slightly reduced, it indicated that the charging and discharging capacity was reduced by doping a small amount of Zn^{2+} and Fe^{3+} , the main reason was that Zn^{2+} and Fe^{3+} were inactive materials. As Li reported that there was no $\text{Mn}^{4+}/\text{Mn}^{3+}$ reduction peak in $\text{Li}[\text{Ni}_{(1/3-x)}\text{Fe}_x\text{Co}_{1/3}\text{Mn}_{1/3}]\text{O}_2$ [6], this discrepancy may be caused by the different doping ways of Fe, Li was doped with iron in the process of coprecipitation, and I was doped with Fe after coprecipitation.

Figure 3b showed that Ti^{4+} doping did not change the oxidation peak potential, while made the reduction potential shift to the left, which indicated that Ti^{4+} doping improved the reversibility of the materials and decreased the polarization in the charging and discharging process. Zr^{4+} doping had little effect on the redox potential of the materials. In Fig. 3b, the three oxidation peaks areas was almost constant, but reduction peak areas of Ti^{4+} doping increased, which illustrated that Ti^{4+} doping may improve the discharge capacity and coulomb efficiency. The reason was that Ti^{4+} doping improved the structural stability of the materials.

3.3 Performance analysis of discharge rate

Fig. 4 showed the third cycle discharge curves of $\text{Li}_{1.05}\text{Co}_{0.3}\text{Ni}_{0.35}\text{Mn}_{0.3}\text{M}_{0.05}\text{O}_2$ ($\text{M}=\text{Zn}$ 、 Fe 、 Ti 、 Zr) materials at different ratios. As shown in Fig4a and table2, the difference of discharge capacity between doped and undoped samples was not significant and the order of the discharge capacity at low current was $\text{Ti}^{4+}\text{-doped} > \text{no doped} > \text{Zr}^{4+}\text{-doped} = \text{Fe}^{3+}\text{-doped} > \text{Zn}^{2+}\text{-doped}$. The discharge capacity of Zn^{2+} -doped, Fe^{3+} doped and Zr^{4+} -doped materials were lower than no doped, because Zn^{2+} , Fe^{3+} and Zr^{4+} was inactive materials. But the increasing discharge capacity of Ti^{4+} doping maybe that Ti^{4+} doping decreased the polarization and improved the conductivity[22].

From Fig4b, Fig4c and table2, under 0.5C rate current discharge, the discharge capacity sequence was $\text{Ti}^{4+}\text{-doped} > \text{Zr}^{4+}\text{-doped} > \text{Zn}^{2+}\text{-doped} = \text{no doped} > \text{Fe}^{3+}\text{-doped}$. under 1C rate current discharge, the discharge capacity changed more obviously and the order was $\text{Ti}^{4+}\text{-doped} > \text{Zr}^{4+}\text{-doped} > \text{Zn}^{2+}\text{-doped} > \text{no doped} > \text{Fe}^{3+}\text{-doped}$. The weakening of the rate discharge capacity and the decrease of the discharge platform with Fe^{3+} -doping was that the impurity phase Li_2MnO_3 appeared and participated in the electrochemical reaction in the Fe^{3+} -doped samples. The improved rate performance of Zn^{2+} -doping, Zr^{4+} -doping and Ti^{4+} -doping samples was due to the partial substitution for transition metal ions to compensate for the vacancy or the loss of electric neutrality causing by the redox of transition metal ions in the charging and discharging process.

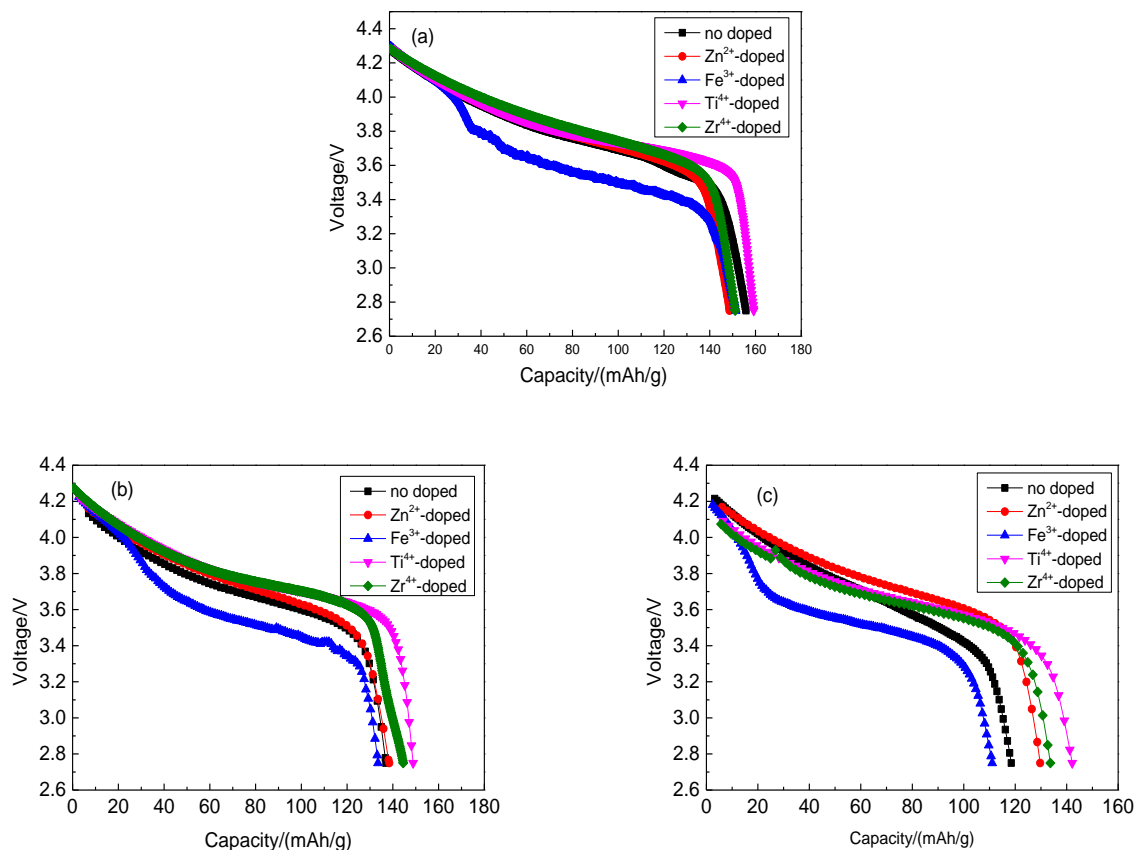


Figure 4. Discharge curves of Li/ $\text{Li}_{1.05}\text{Co}_{0.3}\text{Ni}_{0.35}\text{Mn}_{0.3}\text{M}_{0.05}\text{O}_2$ batteries at different current density (a) 0.1C (b) 0.5C, (c) 1C

Table 2. the discharge capacity of Li/ $\text{Li}_{1.05}\text{Co}_{0.3}\text{Ni}_{0.35}\text{Mn}_{0.3}\text{M}_{0.05}\text{O}_2$ batteries at different current

Materials	the 1 st discharge capacity(mAh/g)			the 3 th discharge capacity(mAh/g)			the 30 th discharge capacity(mAh/g)		
	0.1C	0.5C	1C	0.1C	0.5C	1C	0.1C	0.5C	1C
no doped	157.64	144.54	120.16	155.84	136.95	118.48	146.65	119.88	89.93
Zn-doped	147.64	138.43	129.51	148.65	138.47	129.69	141.71	130.01	119.08
Fe-doped	152.38	133.51	110.34	151.38	133.51	111.07	145.68	126.63	97.45
Ti-doped	159.23	148.82	142.19	159.35	148.88	142.15	154.06	143.69	138.41
Zr-doped	151.54	146.59	133.36	151.14	144.52	133.66	142.59	133.71	127.02

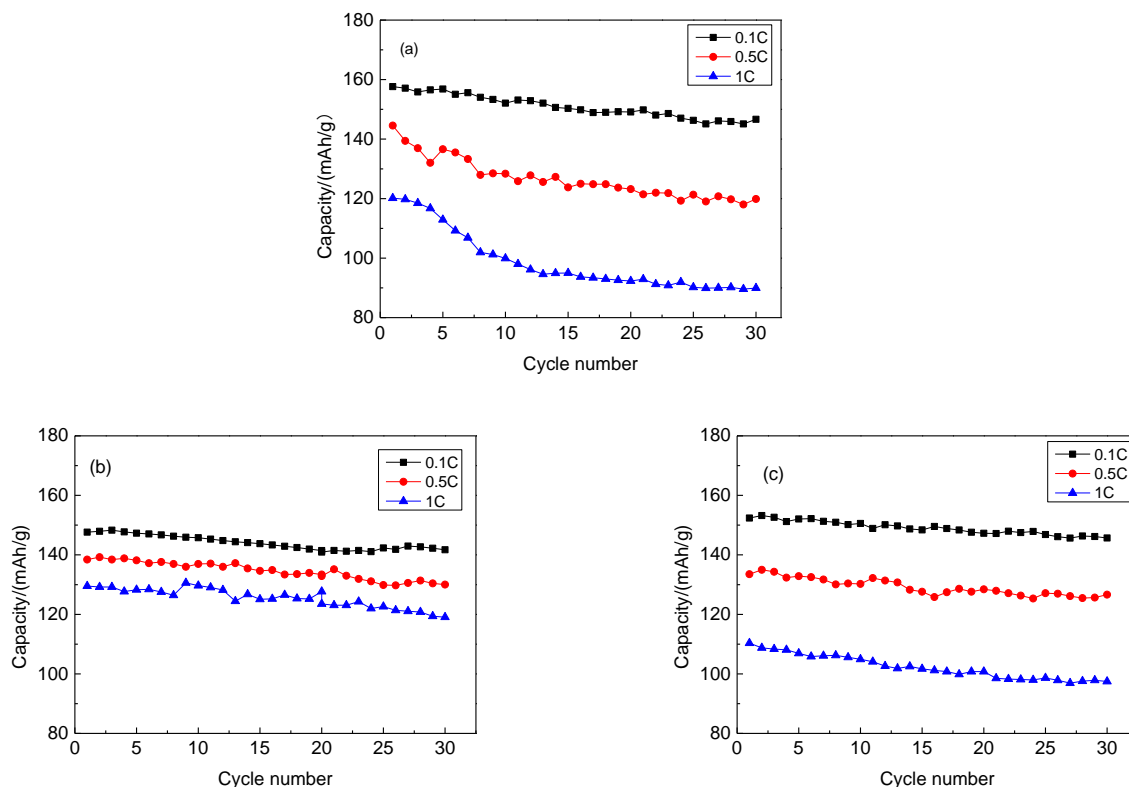
Fig.5 showed cycle performance of Li/ $\text{Li}_{1.05}\text{Co}_{0.3}\text{Ni}_{0.35}\text{Mn}_{0.3}\text{M}_{0.05}\text{O}_2$ cells at high rate discharge. As seen in Fig.5a and table2, the first discharge capability of no doped samples at 0.1C, 0.5C and 1C rate current were 157.64mAh/g,144.54 mAh/g and 120.16mAh/g respectively.The capacity retention rate after 30 cycles were 93.03%, 82.94% and 74.84% respectively. Fig. 5b and table2 showed that the first discharge capability of Zn^{2+} doped samples at 0.1C,0.5C and 1C were 147.64mAh/g,138.43 mAh/g and 129.51mAh/g respectively. The capacity retention after 30 cycles were 95.98%, 93.92% and

91.95% respectively, which indicated that Zn²⁺ doping improved the cyclic stability at high rate. It may be that Zn²⁺ compensated for the vacancy or electric neutral loss causing by the redox of transition metal ions and the polarization decreased.

Fig. 5c showed that the first discharge capacity of Fe³⁺ doped samples at 0.1C,0.5C and 1C rate were 152.38mAh/g,133.51 mAh/g and 110.34mAh/g respectively and the capacity retention after 30 cycles were 95.60%, 94.85% and 88.31% respectively. These results showed that Fe³⁺ doping slightly improved the materials stability under high current discharge, but the effect was not ideal,this result was basically consistent with what Li reported[6].

From Fig. 5d, the discharge capacity of Ti⁴⁺ doped samples at 0.1C, 0.5 C and 1C rate were 159.23 mAh/g, 148.82 mAh/g,142.19 mAh/g and the capacity retention after 30 cycles were 97.09%, 96.55% and 97.34% respectively. The results showed that Ti⁴⁺ doping can improve the materials stability under high current charge-discharge cycles. The reason was that Ti⁴⁺ doping decreased the polarization and improved the conductivity. This result Ti-doped materials was consistent with Ti-NCM111 materials synthesized by Cho[7]

Fig.5e and table 2 showed that the first discharge capacity of at 0.1C, 0.5 C and 1C rate were 159.23 mAh/g,146.59 mAh/g and 133.36 mAh/g and the capacity retention after 30 cycles were 94.09% ,91.21% and 95.24%,which showed that Zr⁴⁺ doping can also improve the stability of high rate cycling. Our results was the same as Zhu[8] reported that the capacity rates of LiNi_{0.83}Co_{0.11}Mn_{0.06}O₂ (NCM) and Zr-NCM were 73.0% and 60.1% respectively.The reason was that Zr doped in NCM can enlarge lattice parameter c and lead to a higher reversible lithium-ion migration rate[21].



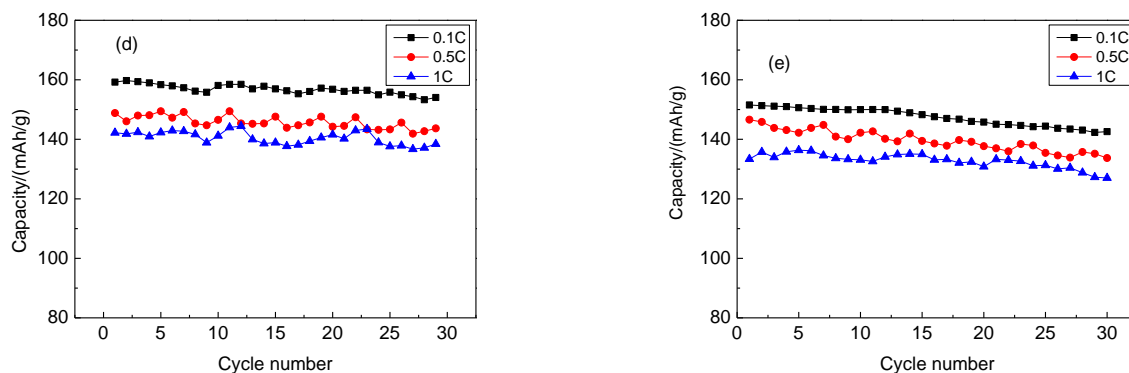


Figure 5. Cycle performance of Li/Li_{1.05}Co_{0.3}Ni_{0.35}Mn_{0.3}M_{0.05}O₂ cells at high rate discharge (a) no doped (b)Zn²⁺-doped, (c) Fe³⁺-doped, (d) Ti⁴⁺- doped, (e) Zr⁴⁺-doped

In conclusion, Zn²⁺, Zr⁴⁺, Ti⁴⁺ (especially Ti⁴⁺) doping can improve the dynamic properties of the materials.

3.4 AC impedance analysis

Figure 6 showed the impedance spectra of Li/Li_{1.05}Co_{0.3}Ni_{0.35}Mn_{0.3}M_{0.05}O₂ cells at 4.2V (vs Li⁺/Li) after 3 weeks cycles. According to Fey’s reports[15],the curves was composed of high frequency semicircle, low frequency semicircle and Warburg impedance. But in Fig.6. the curves were composed of two parts, this difference was due to cells charging state and measurement voltage[22-23]. It was considered that the impedance of the compressed semicircle in this diagram corresponds to the sum of the impedance and the charge transfer impedance of the interface between the lithium ion multilayer film and the solution[15].

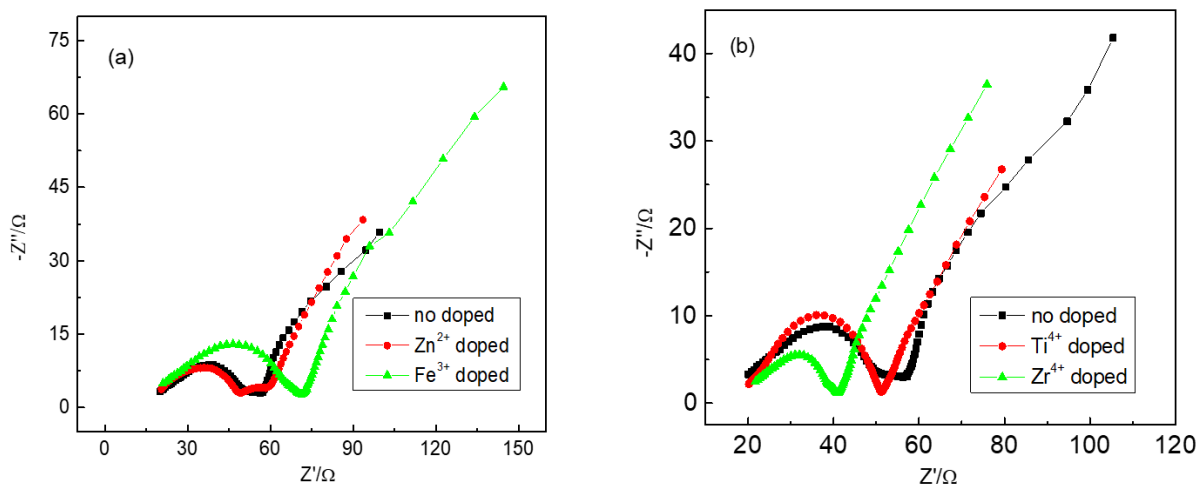


Figure 6. Nyquist plots of Li_{1.05}Co_{0.3}Ni_{0.35}Mn_{0.3}M_{0.05}O₂ (M=Zn, Fe, Ti, Zr) electrodes

The higher the impedance value, the more difficult the electrochemical reaction was, and the charge-discharge capacity and rate performance of the battery may be reduced. As shown in Fig 6, the AC impedance value of Zn^{2+} , Ti^{4+} and Zr^{4+} doped samples were smaller than that of the undoped samples. It was preliminarily believed that Zn^{2+} , Ti^{4+} and Zr^{4+} doping improved the conductivity of electrode materials, so the rate performance of doped materials was improved. However, the impedance value of the Fe^{3+} -doped sample increased and the conductivity of the material deteriorated, so the cycle stability and rate performance were poor.

3.5 Thermal stability studies

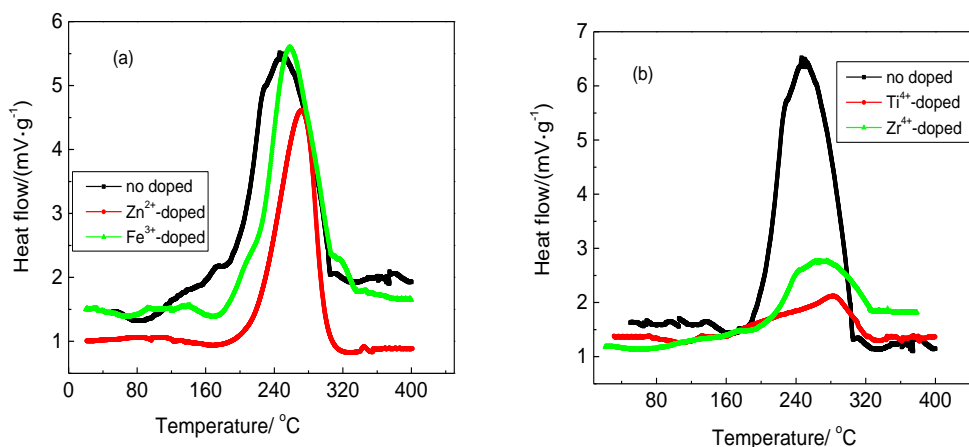


Figure 7. DSC curves of $\text{Li}_{1.05}\text{Co}_{0.3}\text{Ni}_{0.35}\text{Mn}_{0.3}\text{M}_{0.05}\text{O}_2$ ($\text{M}=\text{Zn}, \text{Fe}, \text{Ti}, \text{Zr}$) samples

Fig. 7 was DSC diagrams of a transition metal cation doped samples. As can be seen from the Fig.7, the no doped sample had a weak exothermic reaction at 200°C and reached the maximum exothermic peak at 250°C. The exothermic peak area was the largest among all the diagrams. The initial exothermic temperature of the Zn^{2+} doped samples shifted 20°C to the right and the exothermic peak area was slightly smaller than undoped sample, which indicated that Zn^{2+} doping improved the thermal stability, mainly because Zn^{2+} doping compensated for the vacancy of transition metal and enhanced the structural stability. The initial exothermic temperature of Fe^{3+} -doped samples was not significantly different from that of undoped samples and the maximum temperature of the exothermic peak shifted 10°C to the right. The area of the exothermic peak was slightly smaller than that of undoped samples and the change was not significant. The reason was that the impurity phase deteriorated the molecular structure. The thermal stability of Ti^{4+} and Zr^{4+} doped samples was enhanced and the exothermic area was reduced obviously. The reason was that Ti^{4+} and Zr^{4+} doping compensated the defects of transition metal ions and made the structure of lithium-intercalated materials more stable. By comparison of the two diagrams, it can be seen that the thermal stability order of four doping materials was $\text{Ti}^{4+} > \text{Zr}^{4+} > \text{Zn}^{2+} > \text{Fe}^{3+} = \text{no doped}$.

4. CONCLUSION

Four kinds of metal element doped cathode materials $\text{Li}_{1.05}\text{Co}_{0.3}\text{Ni}_{0.35}\text{Mn}_{0.3}\text{M}_{0.05}\text{O}_2$ (M=Zn, Fe, Ti, Zr) were synthesized by coprecipitation method. The effect of doping was summarized by comparing the structure, morphology, electrochemical properties and thermal stability.

(1) XRD tests showed that $\text{Li}_{1.05}\text{Co}_{0.3}\text{Ni}_{0.35}\text{Mn}_{0.3}\text{M}_{0.05}\text{O}_2$ (M=Zn, Fe, Ti, Zr) had stable layered structure with a-NaFeO₂ type. However, the impurity peaks of ZnO appeared in Zn-doping materials and the impurity peaks Li_2MnO_3 appeared in Fe-doping materials.

(2) The results of CV curves showed that no multiphase reactions appeared and lower polarization in Zn^{2+} , Ti^{4+} or Zr^{4+} doped materials. But in Fe^{3+} doped materials, Li_2MnO_3 took part in the electrochemical reaction and affected the electrochemical properties of the materials.

(3) During 0.1C rate current charge-discharge process, the difference of the discharge capacity and cyclic stability was not significant and the order of the discharge capacity was Ti^{4+} -doped > no doped > Zr^{4+} -doped = Fe^{3+} -doped > Zn^{2+} -doped.

(4) During 0.5C or 1C rate current charge-discharge process, Zn^{2+} , Zr^{4+} , Ti^{4+} (especially Ti^{4+}) doping can enhance the dynamic properties. The order of rate performance and cyclic stability at 1C rate current was Ti^{4+} -doped > Zr^{4+} -doped > Zn^{2+} -doped > no doped > Fe^{3+} -doped.

(5) Zn^{2+} , Ti^{4+} or Zr^{4+} doping delayed the initial temperature and peak temperature of thermal reaction and reduced the heat. The order of the thermal stability was Ti^{4+} -doped > Zr^{4+} -doped > Zn^{2+} -doped > Fe^{3+} -doped = no doped.

ACKNOWLEDGMENT

This work was funded by the project of Hebei Chemical & Pharmaceutical College (No. YZ2022002) and the cultivation of science and technology innovation ability of university and middle school students (No:22E50185D)

References

1. X.Q. Meng, J. Hao, H.B. Cao, X. Lin, P.G. Ning, X.H. Zheng, J.J. Chang, X.H. Zhang, B. Wang and Z. Sun, *Waste Manage.*, 84(2019)54-63.
2. Z.H. Huang, T. Shen, K.Q. Jin, J.H. Sun and Q.S. Wang, *Energy*, 239(2022)121885.
3. Z.G. Wang, H. Luo, H. Liu, F.F. Wu, C.Z. Zhang, Z.X. Wang and P. Yu, *Ceram. Int.*, 47 (2021) 8490-8497.
4. C.F. Yang, J.J. Huang, L.G. Huang and G.J. Wang, *J. Power Sources*, 226 (2013) 219-222.
5. A.K. Budumuru V. Hebbar, M. Viji and C. Sudakar, *Mater. Lett.* X, 11(2021) 10008.
6. H. J. Li, G. Chen, B. Zhang and J. Xu, *Solid State Commun.*, 146(2008)115–120.
7. W. Cho, J.H. Song, K.W. Lee, M.W. Lee, H. Kim, J.S. Yu, Y.J. Kim and K. J. Kim, *J. Phys. Chem. Solids*, 123(2018)271-278.
8. Z.H. Zhu, Y.S. Liang, H. Hu, A. Gao, T. Meng, D. Shu, F.Y. Yi and J.Z. Ling, *J. Power Sources* 498(2021)229857
9. Y.H. Chen, R.Z. Chen, Z.Y. Tang and L. Wang, *J. Alloys Compd.*, 176(2009) 539-542.
10. S.H. Park, S.W. Oh and Y.K. Sun, *J. Power Sources*, 146(2005)622–625.
11. L. F. Jiao, M. Zhang, H.T. Yuan, M. Zhao, J.G. Wei, W. Wang, X.D. Zhou and Y.M. Wang, *J. Power Sources*, 167(2007) 178–184.

12. W.S. Yoon, K.Y. Chung, J. McBreen, X.Q. Yang, *Electrochem. Commun.*, 8(2006) 1257–1262.
13. V. Subramanian and T.K. Fey, *Solid State Ionics*, 148(2002)351-358
14. K.M. Shaju, G.V.S. Rao and B.V.R. Chowdari, *Electrochim. Acta*, 48(2002)145-151.
15. G.T.K. Fey, J.G. Chen, V Subramanian and T Osaka, *J. Power Sources*, 112(2002)384–394.
16. D. T. Liu, Z. H. Wang, L. Q. Chen, *Electrochim. Acta*, 25(2006)4199- 4203.
17. Z. H. Lu, L.Y. Beaulieu, R.A. Donaberger, C. L. Thomas and J.R. Dahn, *J. Electrochem. Soc.*, 149(2002)A778-A791.
18. J. Cho, T.J. Kim, J. Kim, M. Noh and B. Park, *J. Electrochem. Soc.*, 151 (2004)A1899-A1904.
19. K.K. Lee, W.S. Yoon, K.B. Kim, K.Y. Lee, *J. Power Sources*, 97-98(2001)308-312.
20. M. Ganesan, S. Sundararajan, M.V.T. Dhananjeyan, K.B. Sarangapani, N.G. Renganathan, *Mater. Sci. Eng.B*, 131(2006)203-209.
21. K.H. Jeong, H.W. Ha, N.J. Yun, M.Z. Hong, K. Kim, *Electrochim. Acta*, 50(2005)5349–5353.
22. Y.H. Chen, Y.Z. Li, G.Z. Wang, Q. Di, Y.S. Shen, N. Sun and Z.Y. Tang, *Journal of Wuhan University of Technology-Mater. Sci. Ed.*, 27(2012)212-216.
23. P. Sebastien and M. D. Marca, *Electrochem. Commun.*, 6(2004)767–772.

© 2022 The Authors. Published by ESG (www.electrochemsci.org). This article is an open access article distributed under the terms and conditions of the Creative Commons Attribution license (<http://creativecommons.org/licenses/by/4.0/>).